FULL PAPER

Dalton
www.rsc.org/dalton

Molecular structures of $Se(SCH_3)_2$ and $Te(SCH_3)_2$ using gas-phase electron diffraction and *ab initio* and DFT geometry optimisations†

Holger Fleischer,[a] Derek A. Wann,[b] Sarah L. Hinchley,[b] Konstantin B. Borisenko,[b] James R. Lewis,[c] Richard J. Mawhorter,[d] Heather E. Robertson[b] and David W. H. Rankin*[b]

[a] *Institut für Anorganische Chemie und Analytische Chemie, Johannes Gutenberg Universität Mainz, Duesbergweg 10–14, 55099, Mainz, Germany. E-mail: fleische@uni-mainz.de*

[b] *School of Chemistry, University of Edinburgh, West Mains Road, Edinburgh, UK EH9 3JJ. E-mail: d.w.h.rankin@ed.ac.uk*

[c] *Cambridge Astronomy Survey Unit, Institute of Astronomy, Madingley Road, Cambridge, UK CB3 7XT*

[d] *Department of Physics and Astronomy, Pomona College, 610 North College Avenue, Claremont, CA, 91711-6359, USA*

Received 14th April 2005, Accepted 26th July 2005
First published as an Advance Article on the web 24th August 2005

The molecular structures of $Se(SCH_3)_2$ and $Te(SCH_3)_2$ were investigated using gas-phase electron diffraction (GED) and *ab initio* and DFT geometry optimisations. While parameters involving H atoms were refined using flexible restraints according to the SARACEN method, parameters that depended only on heavy atoms could be refined without restraints. The GED-determined geometric parameters (r_{h1}) are: *r*Se–S 219.1(1), *r*S–C 183.2(1), *r*C–H 109.6(4) pm; ∠S–Se–S 102.9(3), ∠Se–S–C 100.6(2), ∠S–C–H (mean) 107.4(5), ϕS–Se–S–C 87.9(20), ϕSe–S–C–H 178.8(19)° for $Se(SCH_3)_2$, and *r*Te–S 238.1(2), *r*S–C 184.1(3), *r*C–H 110.0(6) pm; ∠S–Te–S 98.9(6), ∠Te–S–C 99.7(4), ∠S–C–H (mean) 109.2(9), ϕS–Te–S–C 73.0(48), ϕTe–S–C–H 180.1(19)° for $Te(SCH_3)_2$. *Ab initio* and DFT calculations were performed at the HF, MP2 and B3LYP levels, employing either full-electron basis sets [3-21G(d) or 6-31G(d)] or an effective core potential with a valence basis set [LanL2DZ(d)]. The best fit to the GED structures was achieved at the MP2 level. Differences between GED and MP2 results for *r*S–C and ∠S–Te–S were explained by the thermal population of excited vibrational states under the experimental conditions. All theoretical models agreed that each compound exists as two stable conformers, one in which the methyl groups are on the same side (g^+g^- conformer) and one in which they are on different sides (g^+g^+ conformer) of the S–Y–S plane (Y = Se, Te). The conformational composition under the experimental conditions could not be resolved from the GED data. Despite GED *R*-factors and *ab initio* and DFT energies favouring the g^+g^+ conformer, it is likely that both conformers are present, for $Se(SCH_3)_2$ as well as for $Te(SCH_3)_2$.

Introduction

Spectroscopic and quantum chemical investigations have clearly demonstrated that trisulfane, HSSSH, exists as both *syn* (or g^+g^-) and *anti* (or g^+g^+) conformers, where *syn* and *anti* refer to the positions of the H atoms relative to the S–S–S plane. Due to the small steric demand of the hydrogen atoms, the two conformers differ in energy by only 1 kJ mol^{-1}, in favour of the g^+g^+ conformer.[1] To date only two trisulfane derivatives have been studied using gas-phase electron diffraction. Dimethyl trisulfane, CH_3SSSCH_3, was first studied in 1948,[2] and has recently been reinvestigated,[3] because there were huge uncertainties in the original work. Both conformers of CH_3SSSCH_3 fit the experimental data and it was the small calculated energy difference [7.7 kJ mol^{-1} with MP2(fc)/6-311+g(d) in favour of the g^+g^+ conformer] that led the authors conclude that both were present under the experimental conditions. For bis(trifluoromethyl) trisulfane, CF_3SSSCF_3,[4] the gas-phase electron diffraction data were interpreted on the basis of the g^+g^+ form alone, consistent with a larger *ab initio* energy difference between g^+g^+ and g^+g^- of about 10 kJ mol^{-1} (HF/3-21G*). Structures and conformations of trisulfanes, RSSSR, therefore clearly depend on R.

Our aim was to study the molecular structures of the 2-seleno and 2-telluro derivatives, $Se(SCH_3)_2$ and $Te(SCH_3)_2$, called selenium dimethanethiolate and tellurium dimethanethiolate, respectively. Their molecular structures in the solid state were recently investigated by means of single-crystal X-ray diffraction.[5,6] While $Se(SCH_3)_2$ adopts a g^+g^+ conformation, $Te(SCH_3)_2$ exhibits a g^+g^- conformation in the solid state. In both cases, intermolecular Y···S contacts are present (Y = Se, Te). *Ab initio* calculations suggest that these interactions have an impact on structural parameters and that the effect is more pronounced for $Te(SCH_3)_2$ than for $Se(SCH_3)_2$. GED data should reveal if there are structural differences between the solid and the gaseous states. Furthermore, while structures of molecules composed of light atoms (*e.g.* hydrocarbons) can be very accurately determined by *ab initio* methods,[7] molecules including heavy elements such as selenium and tellurium still pose a challenge for theory. Additionally, little information is available about gas-phase structures of molecules containing selenium or tellurium,[8] and no GED studies have been reported for molecules where the heavier chalcogens (Se, Te) bind to the lighter ones (O, S). The GED structures of $Se(SCH_3)_2$ and

† Electronic supplementary information (ESI) available: Table S1: Nozzle-to-film distances, weighting functions, scale factors, correlation parameters and electron wavelengths, used in the electron diffraction studies of $Se(SCH_3)_2$ and $Te(SCH_3)_2$. Table S2: Comparison of *r*C–C and various amplitudes of vibration for the fractional weight and bilinear methods of digital pixel interpolation for the GED scattering pattern for benzene. Tables S3–S6: Calculated [HF/6-31G(d), B3LYP/6-31G(d), MP2/6-31G(d), MP2/LanL2DZ(d)] coordinates for $Se(SCH_3)_2$. Tables S7–S10: Calculated [HF/3-21G(d), HF/LanL2DZ(d), B3LYP/LanL2DZ(d), MP2/LanL2DZ(d)] coordinates for $Te(SCH_3)_2$. Tables S11 and S12: Least-squares correlation matrix for $Se(SCH_3)_2$ and $Te(SCH_3)_2$. Fig. S1 and S2: Experimental and difference (experimental − theoretical) molecular-scattering intensities for $Se(SCH_3)_2$ and $Te(SCH_3)_2$. See http://dx.doi.org/10.1039/b505287b

DOI: 10.1039/b505287b

$Te(SCH_3)_2$ will thus contribute to the understanding of bonding between heavier and lighter chalcogens and also help to evaluate the quality of the *ab initio* optimised structures.

Experimental

Quantum chemical studies

Quantum chemical *ab initio* and DFT investigations were performed with the Gaussian 98 program package.[9] *Ab initio* geometry optimisations, single-point energy calculations and analytical or numerical calculations of vibrational frequencies were performed at either the HF or the MP2 level. Using DFT methods, a combination of local, gradient-corrected, and exact exchange functionals according to the prescription of Becke[10] and the gradient-corrected correlation functional of Lee, Yang and Parr[11] were employed (B3LYP). The following basis sets were used: a split-valence 3-21G(d) basis set for $Te(SCH_3)_2$,[12] and a split-valence 6-31G(d) basis set for $Se(SCH_3)_2$.[13] The LanL2DZ(d) basis set, used for both $Se(SCH_3)_2$ and $Te(SCH_3)_2$, is made up as follows: Te, Se, S: relativistic effective core potentials (ECP) and the corresponding double-ζ valence basis sets,[14] augmented by appropriate polarisation functions (with exponents according to Höllwarth *et al.*[15]); C: Dunning's and Hay's [3s2p] contracted-valence double-ζ basis,[16] augmented with a set of polarization functions (exponent 0.75); H: Huzinaga's (4s) basis contracted to [2s].[17] Applied symmetry restrictions are given in the text. Force fields were calculated at the MP2/LanL2DZ(d) level. These were used to provide estimates of the amplitudes of vibration (u_{h1}) and the curvilinear corrections (k_{h1}), from the SHRINK program,[18] for use in the gas-phase electron diffraction refinements. Molecular wavefunctions were analysed by means of natural orbitals.[19]

To compare the accuracy of the different theoretical models, a procedure was employed to measure the deviation of calculated geometric parameters from experimental ones. For each of the non-restrained parameters, p_i(C), in the GED refinement of a distinct compound, C, a relative deviation, $\delta_{i,m}$(C) between the GED refined value, $p_{i,\mathrm{GED}}$(C), and the value optimised with a certain model, m [*e.g.* MP2/6-31G(d)], $p_{i,m}$(C), was defined as

$$\delta_{i,m}(\mathrm{C})^2 = ((p_{i,\mathrm{GED}}(\mathrm{C}) - p_{i,m}(\mathrm{C}))/(\mathrm{esd}(p_i))^2/p_{i,\mathrm{GED}}(\mathrm{C})^2 \quad (1)$$

where esd(p_i) is the mean standard deviation of the parameters. They are applied as weighting factors such that a parameter with a large esd has a lower weight.

For each model, m, the overall deviation for a given compound, C, Δ_m(C) is defined as

$$\Delta_m(\mathrm{C}) = \{[\textstyle\sum_i \delta_{i,m}(\mathrm{C})^2]/n(\mathrm{C})^2\}^{1/2} \quad (2)$$

where n(C) is the number of non-restrained geometric parameters for compound C. The smaller Δ_m(C), the more accurate is the model in terms of geometric parameters.

Gas-phase electron diffraction (GED)

Data were collected for $Se(SCH_3)_2$ and $Te(SCH_3)_2$ using the Edinburgh gas-phase electron diffraction apparatus.[20] An accelerating voltage of around 40 kV was used, representing an electron wavelength of approximately 6.0 pm. Scattering intensities were recorded on Kodak Electron Image films at nozzle-to-film distances of 94.89 and 293.46 mm for $Se(SCH_3)_2$ and 97.51 and 259.65 mm for $Te(SCH_3)_2$. In the case of $Te(SCH_3)_2$ both sets of scattering intensity data were recorded with sample and nozzle temperatures held at 348 and 360 K respectively. For $Se(SCH_3)_2$, data were first collected at the longer nozzle-to-film distance, where sample and nozzle temperatures of 286 and 298 K provided a sufficient vaporisation rate for the GED experiment. In order to collect data at the shorter distance it proved necessary to increase the temperatures to 332 and 343 K.

The weighting points for the off-diagonal weight matrices, correlation parameters and scale factors for both camera distances for $Se(SCH_3)_2$ and $Te(SCH_3)_2$ are given in Table S1 (ESI†). Also included are the exact electron wavelengths as determined from the scattering patterns for benzene, which were recorded immediately after the patterns for the sample compounds. The scattering intensities were measured using an Epson Expression 1600 Pro flatbed scanner and converted to mean optical densities as a function of the scattering variable, s, as described in the section below. The data reduction and the least-squares refinement processes were carried out using the ed@ed program[21] employing the scattering factors of Ross *et al.*[22]

Edinburgh scanning software

There are two steps to perform when obtaining scattering information from gas electron diffraction plates or films. Initially the program must find the centre of the scattering pattern, and then it must extract the data from the plate into a digital format that can be used in the ed@ed program.[21]

Centring algorithm

The first step in forming a mean scattering profile is to determine accurately the position of the centre of the scattering pattern. The program does this using a cross-correlation function, as defined in eqn (3), where $f(x)$ is a function and $g(x + h)$ is a similar function, but offset by some amount, h. The program uses a cross-correlation technique in which the displacement between two similar functions can be determined by the convolution integral in eqn (3). $C(h)$ represents the likelihood that the shift between the two functions is h and hence the most likely displacement h' is at the maximum of the function $C(h)$.

$$C(h) = \int [f(x)g(x + h)]\mathrm{d}x \quad (3)$$

With raster data it is necessary to find displacements using a discrete cross-correlation function. The program finds the maximum value of this function and solves for h' by doing a parabolic interpolation near that value.

The simplest way to find the centre of the scattering pattern is to start at an assumed centre of the pattern and cut the raster along both the x axis and the negative x axis, giving two profiles that can be used in the cross-correlation process. The measured shift, h', is an indication of the displacement of the x coordinate of the assumed centre from the true centre of the pattern. If we perform a similar exercise along the positive and negative y axes, then we have an estimate of the location of the true centre in y as well.

Taking this concept one step further, consider a line from the assumed centre at an angle, α, anti-clockwise from the positive x axis, with $0 \leq \alpha \leq 90°$. From this line take four cuts at 90° intervals. Cross-correlate cuts one and three to measure δx, cuts two and four to measure δy. These values are related to the actual displacement of the central coordinates from the assumed centre ($\mathrm{d}x$,$\mathrm{d}y$) by eqns (4) and (5). Doing this over a range of values of α yields a number of estimates of ($\mathrm{d}x$,$\mathrm{d}y$). These can be averaged to form final values $\langle \mathrm{d}x \rangle$ and $\langle \mathrm{d}y \rangle$ as well as an estimate of the scatter about these values. The initial estimate of the central coordinates is updated by adding these mean shifts and then the process repeats until the values of $\langle \mathrm{d}x \rangle$ and $\langle \mathrm{d}y \rangle$ are lower than some preset convergence threshold, which is generally only a fraction of the pixel size.

$$\mathrm{d}x = 0.5[\delta x \cos(\alpha) - \delta y \sin(\alpha)] \quad (4)$$

$$\mathrm{d}y = 0.5[\delta x \sin(\alpha) + \delta y \cos(\alpha)] \quad (5)$$

This method has been adapted and discussed by Weber *et al.*,[23] who have used it in centring their own CCD camera digital electron-diffraction data.

Cross correlation has the advantage that it uses all of the information in the profiles simultaneously and hence gives very robust estimates of displacements. One disadvantage is that the displacement can be severely biased by any low frequencies that are present in the cuts. It is therefore important that such broad features are filtered out before cross correlation. We accomplish this by fitting low-order polynomials and dividing them through the profiles. This ensures that the peaks and troughs of the scattering profile are what determine the centre of the pattern.

Another consideration is the assumption that the data are circular rather than slightly elliptical, in spite of the possible effects of the Earth's magnetic field on the paths of the scattered electrons. A detailed three-component analysis of the situation finds that one component merely rotates the pattern about the beam axis, while the other two cancel because of the geometry of the flat detector intersecting the scattered cone of electrons. Indeed, the data have proved to be circular within the precision of our scanner.

Not all the plate or film is considered when finding the central coordinates of the diffraction pattern, but instead a range of radii is used to define the area to be considered in the cross correlation. The innermost part of the pattern often contains non-ideal data and the image of the beam stop. The user is required to specify the range of radii (in pixel space) that are to be considered in the cross correlation. For raster maps with very low signal it is often worth ignoring much of the outer region of the pattern, as there is very little information there and the noise just increases the random error of the value of the shift.

Profile extraction

Having defined the pattern centre, the second task is to reduce the raster into a mean one-dimensional profile. This is done by azimuthal averaging in concentric rings for each interval in wave number. This latter is defined in eqn (6), where λ_e is the electron wavelength, Δx is the physical pixel size of the raster, r is the radius of the point from the centre of the pattern (in pixels) and Λ_c is the nozzle-to-camera distance. The profiles are calculated over a range of values of s and for a bin size of ds. The value of Δx for our Epson Expression 1600 Pro flatbed scanner was determined from scans of a stellar region.

$$s = \frac{4\pi}{\lambda_e} \sin\left(\frac{1}{2}\arctan\left(\frac{r\Delta_x}{\Lambda_c}\right)\right) \quad (6)$$

Because the raster is discrete rather than continuous, some form of interpolation has to be employed and the program does this in two different ways.

The first method is to use the current value of s to define a value of r, and then sample the raster at this radius at a number of position angles, typically every one degree. The value at a particular radius and position angle is calculated from a bilinear interpolation of the four nearest points to the current values of (x,y). The profile is then taken to be the median value of all the samples at this radius. This method has the advantage that it is very quick.

The second method is to look at all the pixels in the raster. The main issue here is what to do with pixels which fall on the boundaries of the circular bins in s. The method that works best calculates the fractional area of the current pixel that falls into each s bin. That fraction acts as a weight and the final value at that radius is the weighted average of all the pixels that contribute to that bin. This method has the advantage that it uses all of the information in the raster. It is a little slower than the bilinear interpolation method, but not prohibitively so.

With both methods, a CCD background intensity needs to be calculated and subtracted. This CCD background value is calculated in an annulus outside the exposed region of the film.

A detailed study of the bilinear interpolation and fractional weight methods has been carried out on benzene calibration runs at both high temperature and room temperature using both long and short camera distances. The fractional weight method yields better R_G values by about 13% for both sets of short camera distance (larger angle, lower signal-to-noise (S/N) ratio) data, and is better by 3% for the room-temperature long camera distance data. Hence, it is generally preferred. However, the bilinear interpolation method is 8% better for the high-temperature long camera distance experiment. This can be understood because the method (like a traditional densitometer) samples more points that are closer together at small scattering angles with better S/N. Using this small angle data more often gives it more weight and improves the fit, an effect that is smaller but is also in evidence for the better-behaved room-temperature long camera distance data. A table showing this comparison is included in Table S2 (ESI†).

Data transformation

The program allows for several different data formats, and also allows for the data to be in transmission units or in density. As it is density that is wanted, the program can transform a map in transmission as it goes. What is needed is a file with the transformation coefficients. The conversion from transmission to density is modelled for each pixel as a power series expansion of the form given in eqn (7), where x is defined by $x = \log(62000) - \log(\text{transmission})$. The value 62000 is a nominal peak transmission value, set slightly below the notional maximum of 65535 for a scanner using unsigned short integer arithmetic. Higher values will not be observed because there is always some absorption, even for a "clear" object. For other scanners this value may need to be changed.

$$\text{density} = \sum_0^n a_i x_i \quad (7)$$

Results

Ab initio and DFT calculations

Ab initio and DFT investigations were performed at various levels of theory (HF, B3LYP, MP2), employing either full-electron basis sets [3-21G(d) and 6-31G(d)] or an effective core potential with an appropriate valence basis set [LanL2DZ(d); for details see Table 1]. At all levels and with all basis sets employed two conformational energy minima existed for both $Se(SCH_3)_2$ and $Te(SCH_3)_2$, representing conformers with methyl groups in *gauche* positions to the opposite Y–S bond (*i.e.* with ϕSYSC $\cong$ 75–90°). In one case the two groups were on the same side of the S–Y–S plane (g^+g^-) and in the other case they were on opposite sides of the plane (g^+g^+), as shown in Fig. 1. These findings are in accordance with those for HSSSH and CH_3SSSCH_3.[1,3] *Ab initio* optimised molecular geometries and differences in zero-point energies are given in Table 1. Coordinates for these calculated structures are given in Tables S3–S10 (ESI†).

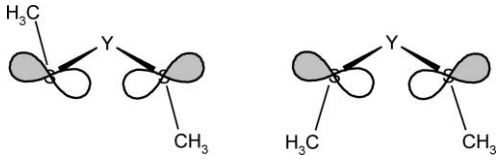

Fig. 1 The g^+g^+ (left) and g^+g^- (right) conformers of $Y(SCH_3)_2$ (Y = Se, Te), showing the p-type lone pairs on the S atoms.

Description of the GED models

On the basis of the MP2/LanL2DZ(d) geometries, a model was written describing the structure of $Se(SCH_3)_2$ as a mixture of both conformers. A similar model was used for $Te(SCH_3)_2$ as the only differences between the Te and Se structures were in the values for the bond lengths, angles and torsions and not in the

Table 1 GED (r_{h1}), XRD and calculated (r_e) geometric parameters for the g^+g^+ (C_2 symmetry) and g^+g^- (C_s symmetry) conformers of $Se(SCH_3)_2$ and $Te(SCH_3)_2$[a,b]

					HF/6-31G(d)		B3LYP/6-31G(d)		MP2/6-31G(d)		MP2/LanL2DZ(d)	
$Se(SCH_3)_2$		GED	Restraint	XRD[c]	C_2	C_s	C_2	C_s	C_2	C_s	C_2	C_s
p_1	rSe–S	219.1(1)	—	218.9(3)	219.1	219.0	222.1	222.0	219.9	219.7	220.9	220.8
p_2	rS–C	183.2(1)	—	180.9(3)	181.7	181.9	183.7	183.9	181.6	181.9	182.7	182.9
p_3	rC–H	109.6(4)	109.6(10)	—	108.1	108.1	109.3	109.3	109.2	109.1	109.6	109.6
p_4	∠S–Se–S	102.9(3)	—	103.2(5)	103.7	105.2	105.4	106.9	103.4	105.6	102.6	105.3
p_5	∠Se–S–C	100.6(2)	—	102.3(6)	101.9	102.8	101.9	102.7	100.4	101.4	101.1	102.4
p_6	∠S–C–H (mean)	107.4(5)	109.2(10)	—	109.3	109.4	109.2	109.3	109.3	109.5	109.2	109.4
p_7	ϕS–Se–S–C	87.9(20)	—	79.8(9)	80.3	89.9	81.3	88.5	78.4	87.7	76.0	88.3
p_8	ϕSe–S–C–H(6)	178.8(19)	179.8(20)	—	183.8	191.2	184.4	193.2	183.1	194.4	179.8	189.1
Δ_m[d]					0.0317		0.0356		0.0221		0.0226	
	ΔE^0[e]				−6.6		−4.9		−6.1		−7.3	

					HF/3-21G(d)		HF/LanL2DZ(d)		B3LYP/LanL2DZ(d)		MP2/LanL2DZ(d)	
$Te(SCH_3)_2$		GED	Restraint	XRD[c]	C_2	C_s	C_2	C_s	C_2	C_s	C_2	C_s
p_1	rTe–S	238.1(2)	—	240.9(3)	240.3	240.3	238.7	238.7	242.0	242.1	239.3	239.3
p_2	rS–C	184.1(3)	—	181.5(5)	182.7	182.8	183.0	183.1	184.9	185.0	183.2	183.5
p_3	rC–H	110.0(6)	109.6(10)	—	108.0	108.0	108.2	108.2	109.5	109.5	109.6	109.6
p_4	∠S–Te–S	98.9(6)	—	98.9(1)	100.4	102.5	101.3	103.2	103.5	105.3	100.3	103.4
p_5	∠Te–S–C	99.7(4)	—	103.8(4)	103.6	104.4	103.7	104.5	103.8	104.3	101.9	102.9
p_6	∠S–C–H (mean)	109.2(9)	109.3(10)	—	109.3	109.5	109.3	109.4	109.3	109.4	109.3	109.5
p_7	ϕS–Te–S–C	73.0(48)	—	85.7(7)	77.2	87.5	78.2	88.5	80.3	88.2	75.7	86.4
p_8	ϕTe–S–C–H(6)	180.1(19)	180.0(20)	—	181.1	186.6	181.3	186.3	182.1	188.3	180.1	187.6
Δ_m[d]					0.0229		0.0223		0.0309		0.0135	
	ΔE^0[e]				−5.1		−6.1		−4.2		−5.5	

[a] Distances (r) are in pm, angles (∠) and torsions (ϕ) in degrees and enthalpies in kJ mol^{-1}. See text for parameter definitions and Fig. 2 for atom numbering. The figures in parentheses are the estimated standard deviations of the last digits. [b] Selected structural parameters of $H_3CSSSCH_3$ from a GED experiment, described in ref. 3 ($r_g/\angle_\alpha$ structure): rS–C 181.7(2), rC–H (mean) 108.4(7) pm; ∠S–S–S 107.3(5), ∠S–S–C 103.1(5), ∠S–C–H (mean) 112(2)°; ϕS–S–S–C 79(5)°. [c] Averaged values over crystallographically different parameters. For XRD structures see refs. 5 [$Se(SCH_3)_2$] and 6 [$Te(SCH_3)_2$]. [d] Δ_m is defined in eqn (2) in the Experimental section and was calculated only for the g^+g^+ conformers. [e] $\Delta E^0 = E^0(C_2) - E^0(C_s)$. E^0 is the sum of electronic and zero-point energies.

general configurations. The geometry of the g^+g^+ conformers was described in terms of eight independent parameters and had overall C_2 symmetry. (See Fig. 2 for atom numbering.) These parameters included three bond lengths, namely rY–S (p_1), rS–C (p_2) and the rC–H value (p_3). A single rC–H value was used because the three individual MP2/LanL2DZ(d) values differed by only 0.3 pm. The model also required three angle parameters, including ∠S–Y–S (p_4) and ∠Y–S–C (p_5). The difference between the largest and smallest value for ∠S–C–H was 4.3° and, in order to account for this asymmetry in the methyl groups, an average S–C–H angle (p_6) was defined and this angle was used in the model in conjunction with fixed (*i.e.* non-refinable) differences to describe the tilt of the methyl groups. (For the Se molecule these fixed differences were −2.6, +1.7 and +0.9°, for the angles to H(6), H(7) and H(8) respectively, and for the Te molecule were −2.9, +1.8 and +1.1°.) The two remaining parameters are dihedral angles. ϕC–S–Y–S (p_7) describes the movement of the S–C bond away from the zero position where it eclipses the opposite Y–S bond. As p_7 was used to describe the torsions on both sides of the molecule, the methyl groups are moved to opposite sides of the SYS plane. The final parameter is ϕY–S–C–H(6/9) (p_8), which describes the torsion of the methyl groups. The calculated structures show that one C–H bond of each group forms a dihedral angle of approximately 180° with the Y–S bond. From this position, a value of less than 180° represents a rotation in a clockwise direction when viewed along the S–C bond towards CH_3.

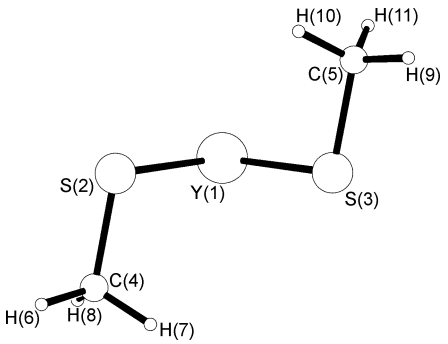

Fig. 2 Gas-phase structure of the g^+g^+ conformer of $Y(SCH_3)_2$ (Y = Se, Te) with atom numbering.

Parameters for the g^+g^- conformers were calculated to be similar to those for the g^+g^+ conformers. Therefore, only the sign of p_7 as applied to the one side of the molecule was changed in the model to preserve C_s symmetry. A non-geometric parameter was also included, allowing the abundance of each conformer to be varied.

With calculations [MP2/LanL2DZ(d)] showing ΔE^0 between g^+g^+ and g^+g^- conformers to be approximately 7.3 kJ mol^{-1} when Y = Se and 5.5 kJ mol^{-1} when Y = Te (see Table 1), the probable abundance of each conformer can be calculated using the Boltzmann distribution at the experimental (nozzle) temperatures. It was predicted that $Se(SCH_3)_2$ would exist with around 85% g^+g^+ and 15% g^+g^- (at 298 K) and 79% g^+g^+ and 21% g^+g^- (at 343 K). In the case of $Te(SCH_3)_2$ the g^+g^+:g^+g^- composition was calculated to be 71 : 29 at 360 K. This already makes it doubtful whether the g^+g^- conformers would be observable in the gas mixture. Another problem is that in terms of the heavy-atom non-bonded distances in both $Se(SCH_3)_2$ and $Te(SCH_3)_2$, the only significant difference that can be expected between the g^+g^+ and g^+g^- conformers is rC···C, which is approximately 80 pm longer for the g^+g^+ conformer. Although rS···C is, in principle, different for the two conformers, the values lie close together and will be found under the same peak in the GED radial-distribution curve. The peaks in the radial-distribution curve represent the distances between pairs of atoms and the areas of these peaks are proportional to the atomic numbers of the pair of atoms and how often that pairing occurs. For molecules containing very heavy atoms, the consequence of this is that distances from the heavy atoms will dominate the radial-distribution curve. This is the case here, where the relative size of the rC···C peak for each conformer is approximately 2% of the size of the largest peak (rSe–S) and this value is even smaller for the tellurium compound.

On performing least-squares refinements for $Se(SCH_3)_2$, using the model that contained both conformers and a non-geometric parameter to control the abundance of each of the conformers in the mixture, the lowest R_G value was found to be when 100(2)% of the g^+g^+ conformer was present. The structure that was returned for the scenario where 100% of the g^+g^- model was present was almost identical (barring rC···C), although the R_G value was higher. The uncertainty associated with the percentage of the g^+g^+conformer was obtained from Fig. 3, where, at a significance level of 95% (for which the R_G ratio is calculated to be 1.016), the value for 2σ was 4%.

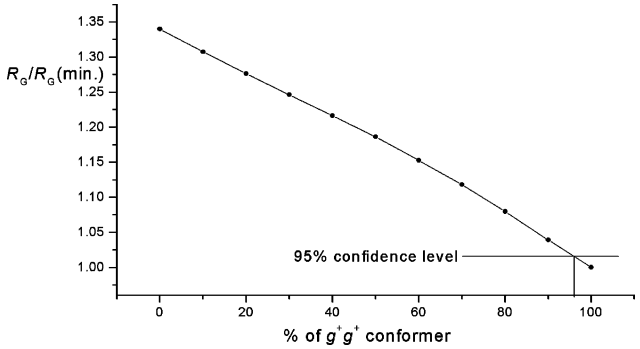

Fig. 3 Variations of R_G ratio with percentage of g^+g^+ conformer of $Se(SCH_3)_2$.

For the refinements using the $Te(SCH_3)_2$ data, the lowest R_G value also resulted from the conformer mix where 100% of the g^+g^+ conformer was present. In this case, however, the value for R_G for 100% of the g^+g^- conformer was only very slightly different. Fig. 4 shows that, at the 95% confidence level, 2σ was 64% and, therefore, the abundance of conformer g^+g^+ in the GED sample was 100(32)%.

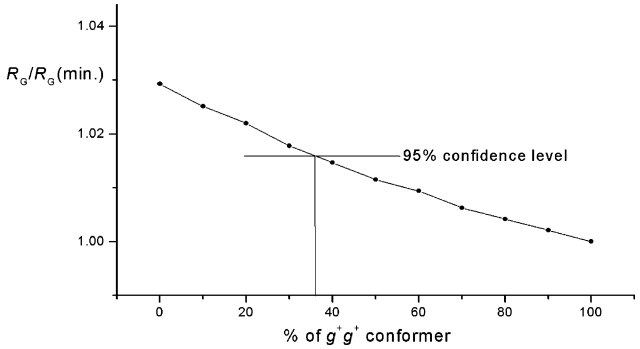

Fig. 4 Variations of R_G ratio with percentage of g^+g^+ conformer of $Te(SCH_3)_2$.

The reported structures of $Se(SCH_3)_2$ and $Te(SCH_3)_2$ will, therefore, be based on g^+g^+ conformers alone.

The processes of refinement for the Se and Te compounds were similar. In both cases eight geometric parameters and seven groups of amplitudes of vibration were refined. (See Table 1 for details of the parameters and Table 2 for the amplitudes of vibration.) For $Se(SCH_3)_2$ flexible restraints were employed, using the SARACEN method,[7,24] for three parameters and three amplitudes. For the purposes of SARACEN, the parameter values were set to be those obtained from calculations performed using the MP2 method with the LanL2DZ(d) basis set on

Table 2 Interatomic distances (r_a) and amplitudes of vibration (u_{h1}) for the restrained GED structures of g^+g^+ $Y(SCH_3)_2$ (Y = Se, Te)[a]

		$Se(SCH_3)_2$			$Te(SCH_3)_2$		
	Atom pair	r_a/pm	u_{h1}/pm[b]	Restraint	r_a/pm	u_{h1}/pm[b]	Restraint
u_1	C(4)–H(8)	109.3(4)	8.4(4)	7.6(8)	110.0(6)	6.5(6)	7.6(8)
u_2	C(4)–H(7)	109.3(4)	8.4 (tied to u_1)	—	110.0(6)	6.6 (tied to u_1)	—
u_3	C(4)–H(6)	109.3(4)	8.4 (tied to u_1)	—	110.0(6)	6.6 (tied to u_1)	—
u_4	H(6)···H(7)	180.5(9)	12.3 (fixed)	—	179.4(14)	12.3 (fixed)	—
u_5	H(6)···H(8)	180.3(9)	12.3 (fixed)	—	179.2(14)	12.3 (fixed)	—
u_6	H(7)···H(8)	178.9(9)	12.1 (fixed)	—	177.6(14)	12.2 (fixed)	—
u_7	S(2)–C(4)	183.3(1)	4.5(2)	—	184.1(3)	5.1(4)	5.2(5)
u_8	Y(1)–S(2)	219.0(1)	5.9(1)	—	238.1(2)	5.5(3)	5.5(6)
u_9	S(2)···H(6)	236.8(8)	11.3 (fixed)	—	240.5(14)	11.4 (fixed)	—
u_{10}	S(2)···H(7)	241.7(11)	10.9 (fixed)	—	244.3(13)	10.9 (fixed)	—
u_{11}	S(2)···H(8)	241.2(11)	10.9 (fixed)	—	244.8(13)	10.9 (fixed)	—
u_{12}	Y(1)···C(4)	309.6(4)	11.1(3)	—	323.6(9)	12.7(7)	10.8(11)
u_{13}	Y(1)···H(7)	315.5(22)	23.3 (fixed)	—	330.4(26)	25.9 (fixed)	—
u_{14}	Y(1)···H(8)	318.9(22)	23.4 (fixed)	—	331.2(26)	25.4 (fixed)	—
u_{15}	S(2)···H(10)	355.5(49)	39.3 (fixed)	—	331.0(129)	48.7 (fixed)	—
u_{16}	S(2)···S(3)	341.9(5)	11.2(3)	—	360.6(16)	13.6(9)	14.0(14)
u_{17}	S(2)···C(5)	404.6(34)	29.2(17)	26.0(26)	391.6(97)	32.7(28)	33.7(34)
u_{18}	Y(1)···H(6)	405.2(5)	11.5 (fixed)	—	422.0(10)	12.3 (fixed)	—
u_{19}	H(7)···H(10)	479.7(105)	57.1 (fixed)	—	398.1(33)	70.7 (fixed)	—
u_{20}	S(2)···H(11)	448.6(47)	35.7 (fixed)	—	430.1(122)	42.9 (fixed)	—
u_{21}	C(4)···H(10)	493.4(81)	48.3 (fixed)	—	430.2(265)	60.6 (fixed)	—
u_{22}	S(2)···H(9)	490.4(33)	30.3 (fixed)	—	480.3(90)	38.4 (fixed)	—
u_{23}	C(4)···C(5)	522.4(61)	35.7(34)	35.7(36)	475.5(207)	46.9(45)	46.4(46)
u_{24}	H(6)···H(10)	550.9(91)	57.6 (fixed)	—	485.0(284)	71.2 (fixed)	—
u_{25}	H(7)···H(11)	557.4(61)	44.2 (fixed)	—	508.9(231)	55.1 (fixed)	—
u_{26}	C(4)···H(11)	576.7(51)	34.6 (fixed)	—	540.5(185)	43.6 (fixed)	—
u_{27}	C(4)···H(9)	592.9(68)	44.4 (fixed)	—	544.3(219)	56.3 (fixed)	—
u_{28}	H(8)···H(11)	616.5(50)	34.3 (fixed)	—	596.3(152)	40.9 (fixed)	—
u_{29}	H(6)···H(9)	657.9(81)	55.8 (fixed)	—	605.0(240)	69.4 (fixed)	—
u_{30}	H(6)···H(11)	654.1(59)	42.3 (fixed)	—	613.8(203)	52.6 (fixed)	—

[a] Estimated standard deviations, as obtained in the least-squares refinement, are given in parentheses. [b] Amplitudes not refined were fixed at the values obtained using the force field calculated at MP2/LanL2DZ(d).

all atoms. Similarly, for $Te(SCH_3)_2$, three parameters were restrained, as well as seven amplitudes of vibration.

The success of the final refinements, for which $R_G = 0.054$ ($R_D = 0.042$) for $Se(SCH_3)_2$, and $R_G = 0.070$ ($R_D = 0.075$) for $Te(SCH_3)_2$, can be assessed on the basis of the radial-distribution and experimental-theoretical difference curves (Fig. 5 and 6) and the molecular-scattering intensity curves (Fig. S1 and S2, ESI†). The least-squares correlation matrices are given in Tables S11 and S12 (ESI†).

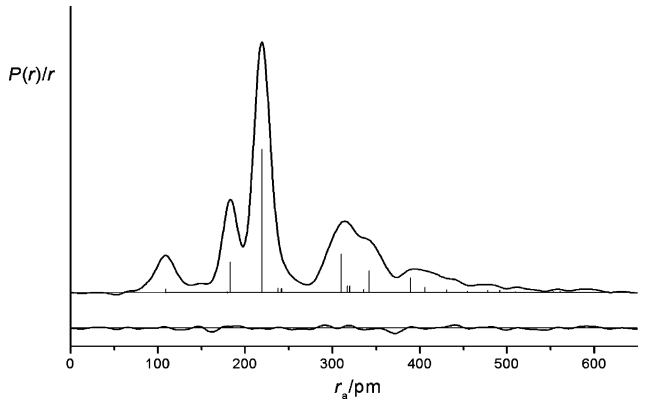

Fig. 5 Experimental radial-distribution curve and theoretical − experimental difference curve for the refinement of $Se(SCH_3)_2$. Before Fourier inversion the data were multiplied by $s\cdot\exp(-0.00002s^2)/(Z_{Se} - f_{Se})(Z_S - f_S)$.

Discussion

A comparison of the gas-phase structures of all three compounds $Y(SCH_3)_2$ (Y = S, Se, Te) reveals several differences between parameters common to all structures. *r*S–C is longest

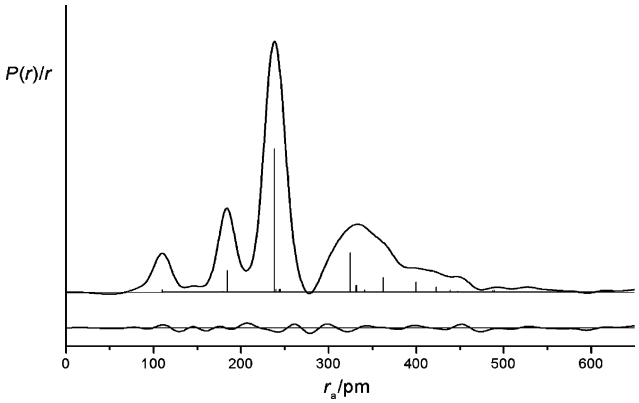

Fig. 6 Experimental radial-distribution curve and theoretical − experimental difference curve for the refinement of $Te(SCH_3)_2$. Before Fourier inversion the data were multiplied by $s\cdot\exp(-0.00002s^2)/(Z_{Te} - f_{Te})(Z_S - f_S)$.

when the central chalcogen atom is heaviest. In order to understand this, *r*S–S, *r*Se–S and *r*Te–S were compared in terms of their bond valences according to O'Keeffe and Brese.[25] The calculated valences increase in the order 1.039 (Y = S) < 1.051 (Y = Se) < 1.132 (Y = Te). It is apparent that the strength of the Y–S bond increases at the cost of the S–C bond. The S–Y–S angles follow an expected trend, becoming smaller as Y becomes heavier. Such a trend has previously been noted, *e.g.* in the series H_2S (92.3°) > H_2Se (91°) > H_2Te (90°).[26] ∠Y–S–C decreases as well when Y becomes heavier, but the differences between angles with different Y atoms are smaller than in the case of ∠S–Y–S. All other common or comparable parameters between the compounds, *i.e.* *r*C–H, ∠S–C–H (mean), ϕS–Y–S–C, and ϕY–S–C–H do not show significant differences. Whether

a conformational mixture is present cannot be resolved with the present GED data and the expected rather small differences between the structural parameters of g^+g^+ and g^+g^- on the basis of their *ab initio* geometries.

$Se(SCH_3)_2$ and $Te(SCH_3)_2$ show several differences between their gas-phase and solid-state structures. While $Se(SCH_3)_2$ shows a significant difference only for *r*S–C, $Te(SCH_3)_2$ reveals differences in *r*Te–S and in *r*S–C (see Table 1). The enlarged Te–S bond in the solid state can be explained by intermolecular Te···S interactions, which involve the n_p(S) and the σ^*(Te–S) orbitals. It should be noted that the XRD experiment was carried out at 133 K,[5] and the difference in bond lengths between the gas and the solid would be even larger if the experiments were done at the same temperature. The Se···S interactions in the solid state are much weaker and consequently *r*Se–S hardly differs between gas and solid states. The difference between *r*S–C in the gas phase and solid state is puzzling and we can offer only a qualitative explanation. A natural bond orbital analysis using the MP2/LanL2DZ(d) model revealed significant n_p(S)–σ^*(C–H) interactions for the two C–H bonds which are *gauche* to the Y–S bond, *i.e.* 90 kJ mol^{-1} for Y = Se (C_2) and 89 kJ mol^{-1} for Y = Te (C_2). n_p(S)–σ^*(C–H) hyperconjugation should strengthen and shorten the S–C bond. Since this interaction depends on the torsion angle around the S–C bond, *r*S–C and the relative energy of the molecules is expected to be a function of ϕY–S–C–H, and this can be shown by a potential energy surface scan (see Fig. 7). The energy minima correspond to the shortest S–C bonds (182.6 pm for Y = Se and 183.2 pm for Y = Te) and the maxima to the longest (183.6 pm for Y = Se and 184.1 pm for Y = Te). An explanation for the lengthening of the S–C bonds in the gas phase can be given on the basis of Fig. 7. At the temperatures of the GED experiment, the CH_3 group should rotate effectively freely around the S–C bond and the S–C bond length adopts an average value. In the solid state at 133 K, the rotation of the methyl group can be assumed to be hindered, thus the average torsion angle is closer to the minimum value and the S–C bond is consequently shorter.

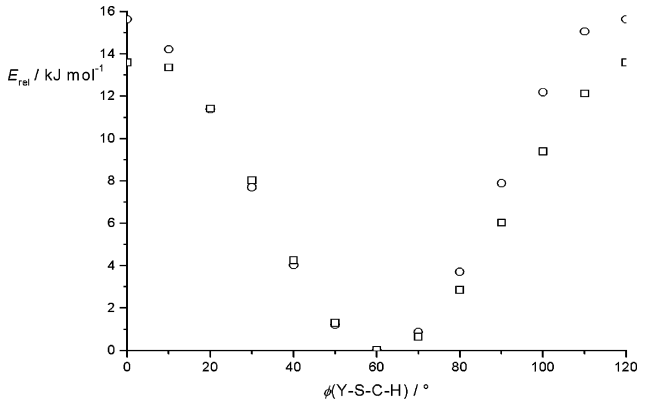

Fig. 7 Relative energies of $Se(SCH_3)_2$ (○, C_2) and $Te(SCH_3)_2$, (□, C_2) as a function of ϕY–S–C–H (Y = Se, Te).

On the other hand, the optimised S–C bond lengths, which refer to r_e structures at 0 K, are longer than observed in the solid state at all levels of theory. This result points to an effect of the solid state on S–C, but this bond shrinkage cannot be explained by dipolar forces in the solid state, since calculated variations in dipole moments with *r*S–C are too small to account for the effect.

Comparison of theoretical models

The energy differences between the g^+g^+ and g^+g^- conformers obtained at different levels of theory follow the same trend as found for $H_3CSSSCH_3$,[3] *i.e.* HF > MP2 > B3LYP, with the difference between HF and MP2 being smaller than that between MP2 and B3LYP. Concerning the accuracy of geometric parameters, measured in terms of Δ_m(C) (see eqn 2), the density functional method performs the least well for both $Se(SCH_3)_2$ and $Te(SCH_3)_2$, with the exception of the *r*S–C parameter, which is best reproduced at the B3LYP level. A comparison of full-electron basis sets and the ECP-valence basis set shows that both have a comparable performance, either 3-21G(d) and LanL2DZ(d) at the HF level or 6-31G(d) and LanL2DZ(d) at the MP2 level. The best agreement between theory and experiment is found at the MP2 level. The smaller value of ∠S–Te–S found in the GED experiment when compared to the *ab initio* optimised geometries is explained by the thermal excitation of torsional vibrations. In both the g^+g^+ and g^+g^- conformers, the p-type lone pairs on the sulfur atoms point towards each other (see Fig. 1) and their mutual repulsion widens the S–Te–S angle. An MP2/LanL2DZ(d) optimisation of $Te(SCH_3)_2$ with C_{2v} symmetry ("W-shaped" CSTeSC skeleton) confirms this explanation. The p-type lone pairs of the sulfur atoms do not repel each other under that symmetry and ∠S–Te–S is subsequently smaller (91.2°).

Acknowledgements

D. A. W. would like to thank the EPSRC and School of Chemistry for funding a studentship.

References

1 M. Liedtke, A. H. Saleck, K. M. T. Yamada, G. Winnewisser, D. Cremer, E. Kraka, A. Dolgner, J. Hahn and S. Dobos, *J. Phys. Chem.*, 1993, **97**, 11204.
2 J. Donohue and V. Schomaker, *J. Chem. Phys.*, 1948, **16**, 92.
3 Q. Shen, C. Wells and K. Hagen, *Inorg. Chem.*, 1998, **37**, 3895.
4 M. Gaensslen, R. Minkwitz, W. Molzbeck and H. Oberhammer, *Inorg. Chem.*, 1992, **31**, 4147.
5 H. Fleischer, S. Glang, N. W. Mitzel, D. Schollmeyer and M. Bühl, *Dalton Trans.*, 2004, 3765.
6 H. Fleischer, N. W. Mitzel and D. Schollmeyer, *Eur. J. Inorg. Chem.*, 2003, 815.
7 N. W. Mitzel and D. W. H. Rankin, *J. Chem. Soc., Dalton Trans.*, 2003, 3650.
8 K. B. Borisenko, B. M. Broschag, I. Hargittai, T. M. Klapotke, D. Schroeder, A. Schulz, H. Schwarz, I. C. Tornieporth-Oetting and P. S. White, *J. Chem. Soc., Dalton Trans.*, 1994, 2705; A. J. Blake, C. R. Pulham, T. M. Greene, A. J. Downs, A. Haaland, H. P. Verne, H. V. Volden, C. J. Marsden and B. A. Smart, *J. Am. Chem. Soc.*, 1994, **116**, 6043; P. Maggard, V. A. Lobastov, L. Schaefer, J. D. Ewbank and A. A. Ischenko, *J. Phys. Chem.*, 1995, **99**, 13115; A. Haaland, H. P. Verne, H. V. Volden and J. A. Morrison, *J. Am. Chem. Soc.*, 1995, **117**, 1554; A. Kovács, 1997, 1037; K.-G. Martinsen and R. J. M. Konings, *J. Chem. Soc., Dalton Trans.*, 1997, 1037; A. Haaland, D. J. Shorokhov, H. V. Volden, H. J. Breunig, M. Denker and R. Rösler, *Z. Naturforsch., Teil B*, 1998, **53**, 381.
9 M. J. Frisch, G. W. Trucks, H. B. Schlegel, G. E. Scuseria, M. A. Robb, J. R. Cheeseman, V. G. Zakrzewski, J. A. Montgomery, Jr., R. E. Stratmann, J. C. Burant, S. Dapprich, J. M. Millam, A. D. Daniels, K. N. Kudin, M. C. Strain, O. Farkas, J. Tomasi, V. Barone, M. Cossi, R. Cammi, B. Mennucci, C. Pomelli, C. Adamo, S. Clifford, J. Ochterski, G. A. Petersson, P. Y. Ayala, Q. Cui, K. Morokuma, D. K. Malick, A. D. Rabuck, K. Raghavachari, J. B. Foresman, J. Cioslowski, J. V. Ortiz, A. G. Baboul, B. B. Stefanov, G. Liu, A. Liashenko, P. Piskorz, I. Komaromi, R. Gomperts, R. L. Martin, D. J. Fox, T. Keith, M. A. Al-Laham, C. Y. Peng, A. Nanayakkara, C. Gonzalez, M. Challacombe, P. M. W. Gill, B. G. Johnson, W. Chen, M. W. Wong, J. L. Andres, M. Head-Gordon, E. S. Replogle and J. A. Pople, *Gaussian 98 (Revision A.6)*, Gaussian, Inc., Pittsburgh, PA, 1998.
10 A. D. Becke, *J. Chem. Phys.*, 1993, **98**, 5648.
11 C. Lee, W. Yang and R. G. Parr, *Phys. Rev. B*, 1988, **37**, 785.
12 J. S. Binkley, J. A. Pople and W. J. Hehre, *J. Am. Chem. Soc.*, 1980, **102**, 939; M. S. Gordon, J. S. Binkley, J. A. Pople, W. J. Pietro and W. J. Hehre, *J. Am. Chem. Soc.*, 1982, **104**, 2797; K. D. Dobbs and W. J. Hehre, *J. Comput. Chem.*, 1986, **7**, 359.
13 P. C. Hariharan and J. A. Pople, *Theor. Chim. Acta*, 1973, **28**, 213; M. M. Francl, W. J. Pietro, W. J. Hehre, J. S. Binkley, M. S. Gordon, D. J. DeFrees and J. A. Pople, *J. Chem. Phys.*, 1982, **77**, 3654; R. C. Binning, Jr. and L. A. Curtiss, *J. Comput. Chem.*, 1990, **11**, 1206.

14 W. R. Wadt and P. J. Hay, *J. Chem. Phys.*, 1985, **82**, 284.
15 A. Höllwarth, M. Böhme, S. Dapprich, A. W. Ehlers, A. Gobbi, V. Jonas, K. F. Köhler, R. Stegmann, A. Veldkamp and G. Frenking, *Chem. Phys. Lett.*, 1993, **208**, 237.
16 T. H. Dunning and P. J. Hay, in *Modern Theoretical Chemistry, Vol. 4*, ed. H. F. Schaefer, Plenum Press, New York, 1977, pp. 1–27.
17 T. H. Dunning, *J. Chem. Phys.*, 1970, **53**, 2823; T. H. Dunning, *J. Chem. Phys.*, 1971, **55**, 716.
18 V. A. Sipachev, *J. Mol. Struct. (THEOCHEM)*, 1985, **121**, 143; V. A. Sipachev, *J. Mol. Struct.*, 2001, **567–568**, 67.
19 A. E. Reed, R. B. Weinstock and F. Weinhold, *J. Chem. Phys.*, 1985, **83**, 735; A. E. Reed, L. A. Curtiss and F. Weinhold, *Chem. Rev.*, 1988, **88**, 899.
20 C. M. Huntley, G. S. Laurenson and D. W. H. Rankin, *J. Chem. Soc., Dalton Trans.*, 1980, 954.
21 S. L. Hinchley, H. E. Robertson, K. B. Borisenko, A. R. Turner, B. F. Johnston, D. W. H. Rankin, M. Ahmadian, J. N. Jones and A. H. Cowley, *Dalton Trans.*, 2004, 2469.
22 A. W. Ross, M. Fink and R. Hilderbrandt, *International Tables for Crystallography, Volume C*, ed. A. J. C. Wilson, Kluwer Academic Publishers, Dordrecht, Netherlands, 1992, p. 245.
23 J. D. Cardoza, R. C. Dudek, R. J. Mawhorter and P. M. Weber, *Chem. Phys.*, 2004, 307.
24 A. J. Blake, P. T. Brain, H. McNab, J. Miller, C. A. Morrison, S. Parsons, D. W. H. Rankin, H. E. Robertson and B. A. Smart, *J. Phys. Chem.*, 1996, **100**, 12280; P. T. Brain, C. A. Morrison, S. Parsons and D. W. H. Rankin, *J. Chem. Soc., Dalton Trans.*, 1996, 4589.
25 M. O'Keeffe and N. E. Brese, *J. Am. Chem. Soc.*, 1991, **113**, 3226.
26 N. Wiberg, *Hollemann–Wiberg, Lehrbuch der Anorganischen Chemie*, Walter de Gruyter, Berlin, New York, 101st edn, 1995.